Journal of Constructional Steel Research 93 (2014) 107–118

Contents lists available at ScienceDirect

Journal of Constructional Steel Research

Fire design of steel columns: Effects of thermal gradients

Anil Agarwal [a,*], Lisa Choe [b], Amit H. Varma [c]

[a] Bentley Systems, Inc., Exton, PA 19341, United States
[b] Research Structural Engineer, NIST, Gaithersburg, MD 20877, United States
[c] School of Civil Eng., Purdue University, West Lafayette, IN 47907, United States

ARTICLE INFO

Article history:
Received 14 June 2013
Accepted 31 October 2013
Available online xxxx

Keywords:
Columns
Fire
Thermal gradient
Elevated temperature
Column design
Beam-column

ABSTRACT

The behavior and design of steel columns subjected to thermal gradients due to fire loading were evaluated numerically and experimentally. The numerical (FEM) modeling approach was verified using experimental data from large-scale tests. The FEM modeling approach was used to conduct parametric studies to evaluate the effects of different heating configurations on steel column strength, and failure behavior at elevated temperatures. The analyses were conducted by coupling transient heat transfer analysis with implicit dynamic stress analysis. Columns subjected to four sided heating configuration had uniform temperature distributions through the cross-section. The columns were subjected to non-uniform (partial) heating to produce thermal gradients through the cross-section. The analysis results indicated that the column strength and failure behavior depended on the column slenderness, axial loading, and heating configuration. Failure modes included flexural buckling about the weak axis, flexural buckling about the strong axis, and flexural-torsional buckling. The analysis results also indicated that columns subjected to uniform heating had significantly higher heat influx. In most cases, columns subjected to non-uniform heating failed at lower average temperatures than columns subjected to uniform heating. However, the columns subjected to uniform heating reached their failure temperatures faster than the columns subjected to non-uniform heating due to the higher heat influx. The exceptions were very slender columns subjected to axial loads greater than 50% of their ambient load capacity. The results from the parametric studies were used to develop design equations for wide flange steel columns subjected to non-uniform heating resulting in thermal gradients through the cross-section.

1. Introduction

Current design guidelines for steel columns in fire conditions are based on assumptions that may not be true for columns in a real building fire. Uniform temperature distribution is one of the most significant assumptions that can potentially lead to overestimation of column load capacity.

The American Institute of Steel Construction [AISC] guidelines [1] for designing steel columns at elevated temperatures were originally proposed by Takagi and Deierlein [2]. The AISC equation (A-4-2) calculates the strength limit state of steel columns at elevated temperatures and accounts for the inelastic flexural buckling mode of failure of wide-flange steel columns. The AISC equation is based on the steel yield stress (F_y^T) and elastic modulus (E^T) values at elevated temperatures similar to those in Eurocode-3 [3]. Agarwal and Varma [4] have proposed another set of design guidelines, wherein they recommended the use of the AISC [1] column design curves at ambient temperature along with a set of calibrated steel yield stress (F_y^T) and elastic modulus (E^T) values. Current column design equations in Eurocode-3 [3] were proposed by Talamona et al. [5]. All these design equations assume that the columns are heated uniformly. This assumption may not necessarily be true for real compartment fires such as perimeter columns, which are more likely to be heated from one side, producing thermal gradients in the column cross-section.

Columns can have non-uniform temperature distributions through their cross-sections and along their length. Temperature variations along the length are ignored in the design process for the following reasons:

(i) Post-flashover fires are assumed to cause sufficient turbulence and mixing of hot gases to maintain uniform temperature through the height of the compartment. A number of popular post-flashover fire models (e.g., Swedish [6], COMPF2 [7], OZONE [8], and Lie [9]) for predicting the compartment fire temperatures are based on the assumption of a single-zone model, wherein the gas temperature inside the compartment is assumed to be uniform. The parametric air Temperature–time (T–t) curve prescribed by the Eurocode-1 [10] is also based on a single-zone model.

* Corresponding author at: 515 Mullica Hill Rd., A209, Glassboro, NJ 08028, United States.
E-mail addresses: anilagar001@gmail.com (A. Agarwal), lisa.choe@nist.gov (L. Choe), ahvarma@purdue.edu (A.H. Varma).

0143-974X/$ – see front matter © 2013 Elsevier Ltd. All rights reserved.
http://dx.doi.org/10.1016/j.jcsr.2013.10.023

(ii) The geometric properties of both columns and fire protection are uniform along the length. This helps with uniform temperature distribution along the column length.
(iii) Assigning the temperatures of the hottest cross-section to the entire column length is considered a conservative assumption.

It may not always be safe to assume uniform temperature distribution across the column cross-section. Olawale [11], Garlock and Quiel [12], and Antonio et al. [13] have shown that a column designed using uniform temperature distribution across the cross-section may not be safe when only one side of the column is exposed to fire. They used numerical schemes to demonstrate that columns with thermal gradient across the column cross-section may fail when the average temperature of the column is lower than the failure temperature of columns heated uniformly.

Thermal gradient across a column cross-section has the following consequences: (1) the hotter side of the column expands more than the cooler side, making the column bow towards the hotter side. This is referred to as the bowing effect. When coupled with the axial compressive load acting on the column, it produces a secondary moment that may cause an increase in compression on the cooler side, and a reduction in compression on the hotter side of the column. (2) The column cross-section becomes structurally asymmetric because the mechanical properties of steel (e.g., yield stress and elastic modulus) are temperature dependent. Garlock and Quiel [14] have presented a detailed discussion on the structural asymmetry produced by the uneven heating of the column cross-section. They have shown that the effective centroid (location of the instantaneous neutral axis) shifts towards the cooler side of the cross-section and that this shift of the neutral axis coupled with the compressive axial load produces a bending moment causing an increase in compression on the hotter side and a reduction in compression on the cooler side of the cross-section, making the column bend towards the cooler side. The shift of the effective centroid does not depend on the length of the column. However, as the axial load applied on the column increases, the bending moment increases too. Garlock and Quiel [14] have also pointed out that the bowing effect causes an increase in compression on the cooler side, and the shift in the neutral axis causes an increase in compression on the hotter side, and the two effects are not additive.

Most of the research work (experimental and analytical) conducted on steel columns at elevated temperatures focuses on uniformly heated columns, e.g., Olesen [15], Vandamme and Janss [16], Aasen [17], Janss and Minne [18], and Franssen et al. [19]. A few efforts to develop design guidelines for a steel column with a thermal gradient are discussed here.

Garlock and Quiel [12] used a fiber-based approach to develop an axial force–moment (P–M) interaction curve for a wide-flange column cross-section exposed to uneven heating and compared the results with the case of uniform heating. The study concluded that: (1) the thermal gradient in a column can alter the plastic P–M interaction curve significantly and that (2) the assumption of uniform temperature distribution can give an unconservative estimate of the section capacity. Using the methodology and findings of this research, Quiel and Garlock [20] have also developed a numerical scheme for predicting the thermal and structural response of a perimeter column (potentially having thermal gradient) subjected to fire.

Dwaikat et al. [21] conducted fire tests on four steel columns subjected to thermal gradient. The tests were conducted in a furnace and uniform heating was applied from all sides. In order to induce thermal gradient in the column cross-section, fire protection was partially removed from surfaces of the specimens. The columns were fixed against rotation and translation at one end and partially restrained against rotation and translation at the other end. The setup was designed to imitate loading conditions similar to that of a column in a Moment Resisting Frame (MRF). It was observed that, due to the thermal gradient, the columns behaved like a beam-column. Load level, fire scenario, and the direction of the thermal gradient were found to have a significant influence on the fire response of such columns. Dwaikat and Kodur [22] used a combination of fiber-based analysis of the column cross-section and detailed FE analysis to develop an equation for calculating the capacity of beam-columns with thermal gradient effects. The equation proposed by Dwaikat and Kodur [22] is a modified version of the current AISC design equations for beam-columns at ambient temperature. Further, the capacity of a W14 × 176 column with a thermal gradient along the web calculated by detailed FE analysis was compared with the capacity calculated using the proposed equation. It was found that the proposed equation offers a better estimate of the capacity than the beam-column design equations meant for uniformly heated columns. This study focused on the inelastic flexural buckling mode of failure. It was based on the analysis of columns with ends restrained against rotation. These equations need to be calibrated and potentially modified for simply supported members and for the possibility of flexural torsional buckling mode. A more detailed validation study should be conducted to ensure that the proposed equation works for columns with various sizes, load levels, levels of heating, and magnitudes and both directions of the thermal gradient.

Choe [23] has conducted full scale column tests at elevated temperatures with thermal gradient along the flange width. The column flanges were heated using a number of ceramic fiber radiation heaters. Individual heaters were controlled independently and were assigned different target temperature–time (T–t) histories to induce the desired level of heat flux at different locations on the column surface. In comparison to a furnace test, this setup allows better control over temperature distribution in a column cross-section. Table 1 summarizes the test matrix for the three column specimens SP1, SP2 and SP3. In the table, L/r_y is slenderness ratio in the weak axis, P^T_u is an imposed axial load, P^{20}_u is an axial load capacity of a column at ambient temperature, and $T_{eq,\ uniform}$ is the failure temperature of an equivalent column heated uniformly. The values of $T_{eq,\ uniform}$ were obtained from another set of tests conducted on similar columns heated uniformly and reported by Choe et al. [24]. The findings of these tests are used as benchmarks to validate the numerical analysis scheme developed and the column design equation proposed in this paper.

The objective of this paper is to explore the possible modes of failure of a steel column exposed to uneven heating and to identify and quantify various factors that control the load capacity, behavior, and failure mode of such columns. A design equation similar to the one proposed by Dwaikat and Kodur [22] has been proposed for a pin-ended column that accounts for pure flexural as well as flexural-torsional buckling modes of column failure. This equation is validated for columns of different sizes and slenderness values with the two different directions of thermal gradient and various levels of heating and loading.

Table 1
Test matrix of the column tests with thermal gradient (Choe [23]).

Specimen	L/r_y	Direction of thermal gradient	SFRM	P^T_u (kN)	P^T_u/P^{20}_u	Failure temperature (°C)			
						T_{max}	T_{min}	T_{avg}	$T_{eq,\ uniform}$
SP1-W8 × 35	69	Along flanges	Full	800	0.4	570	480	550	600
SP2-W14 × 53	71	Along flanges	Full	1450	0.67	470	390	430	500
SP3-W14 × 53	71	Along flanges	Partial	1450	0.67	430	270	340	500

2. Modeling and validation

The Finite Element Method (FEM) was used to numerically investigate the effects of thermal gradients on the behavior, load capacity, and failure mechanism of wide flange steel columns. A detailed parametric study was performed on columns of various sizes and heating configurations to determine their failure mechanisms and load capacities. The numerical investigations indicate that depending upon the level of axial loads and thermal loading, axially loaded columns subjected to thermal gradients are likely to behave similar to a beam-column of an asymmetric cross-sections subjected to combined axial force and bending moment. The results from the parametric studies are used in this paper to: (i) explain the behavior and failure mechanisms of wide flange steel columns subjected to different heating configurations, (ii) develop a design methodology that can be used with current steel design specifications, and (iii) design and conduct a limited experimental validation.

The numerical investigations were conducted in two sequential steps: (1) heat transfer analysis and (2) structural analysis. The heat transfer analysis was conducted to simulate the effects of three hypothetical cases of fire exposure on wide flange steel columns, namely: (1) uniform heating, (2) heating to develop thermal gradient along the web, and (3) heating to develop thermal gradient along the flanges. The results were used to develop temperature profiles through the cross-section for the duration of the fire. The temperature variations along the column length are assumed to be negligible, which permitted a two-dimensional heat transfer analysis of the column cross-section. The temperature profiles developed from the heat transfer analysis are used in structural analysis to determine the structural response of the column subjected to axial loading. Commercially available finite element software, ABAQUS [25] was used for both of these analyses.

2.1. Heat transfer analysis

2.1.1. Modeling and material properties

Two-dimensional finite element models of W-shape steel column cross-sections were developed. Steel columns are typically protected with Spray-applied Fire Resistive Material (SFRM). The thermal properties of SFRM vary among manufacturers. As noted in the AISC Steel Guide 19 [26], representative values for thermal conductivity, mass density, and specific heat of the fire protection material may be taken as 0.135 W/m-K, 293 kg/m^3, and 754 J/kg-K, respectively. Temperature dependent thermal properties of structural steel are taken as specified in the Eurocode-3 [3]. Heat transfer analysis accounts for heat transfer through convection and radiation between air and the exposed surface of the fire protection, and conduction within the SFRM and steel. The column cross-section and the surrounding fire protection were modeled using 2-D, 4-noded, rectangular heat transfer elements DC2D4.

2.1.2. Analysis scheme

Heat transfer within solid elements takes place through conduction alone. Heat flux through conduction (q_c) is given by Eq. (1), where (∇T) is the temperature gradient in 2-dimensioanl space and (k) is the thermal conductivity of the material. Heat flux between gas and the solid surface (q_f) is given by Eq. (2), where T_g is the gas temperature and T_s is the surface temperature, and h_f is the effective film coefficient given by Eq. (3), where h_c and h_r are the heat transfer coefficients for convection and radiation, respectively. Eurocode-1 [10] recommends a constant value of h_c equal to 25 W/m^2.K for surfaces exposed to standard fire. The radiation coefficient (h_r) was determined using Eqs. (4) and (5), where ε_g and α_g are the total gas emissivity and absorptivity calculated using empirical equations proposed by Wong [27], and ε_{eq} is the effective emissivity calculated using the gas (T_g) and surface temperatures (T_s). Stefan–Boltzmann constant (σ) is equal to 5.67 × 10^{-8} W/m^{2}K^4.

$$q_c = -k(\nabla T) \tag{1}$$

$$q_f = h_f\left(T_g - T_s\right) \tag{2}$$

$$h_f = h_c + h_r \tag{3}$$

$$h_r = \varepsilon_{eq}\sigma\left(T_g^2 + T_s^2\right)\left(T_g + T_s\right) \tag{4}$$

$$\varepsilon_{eq} = \frac{\varepsilon_g T_g^4 - \alpha_g T_s^4}{T_g^4 - T_s^4} \tag{5}$$

Detailed validations for this analytical procedure have been presented by Cedeno et al. [28] in the context of a composite floor system. There is no fundamental difference between the heat transfer analysis of a column cross-section and a composite beam cross-section.

2.2. Structural analysis

The structural analysis was conducted using the modeling approach developed and validated by Agarwal and Varma [4]. The steel columns were modeled using four-node shell (S4R) elements with reduced integration. The column cross-section had several (19–20) nodes and at least six square elements across the width of each flange. The initial imperfection (length/1500) and residual stresses in the column (calibrated to match the maximum residual stress value to 30% of the ambient yield strength of steel) were explicitly modeled. Temperature dependent material properties like the σ–ε–T relationship and the thermal expansion coefficient (α) of steel were based on those provided in Eurocode-3 [3].

The structural analysis was conducted by subjecting the columns to axial loading followed by heating. The axial loading was applied using a static analysis approach and maintained constant while the model was subjected to heating using the nodal T–t histories calculated by the heat transfer analysis. The structural analysis for the heating phase was conducted using the implicit dynamics analysis approach with modified Newton–Raphson iteration. The details of this model and the validation of this scheme for uniformly heated columns have been presented by Agarwal and Varma [4] and are not being repeated here for brevity. However, the applicability of this scheme for steel columns with thermal gradients is validated against the column tests conducted by Choe [23] and is presented in the following subsection.

2.3. Column tests and validation of the numerical scheme

As discussed earlier, column tests shown in Table 1 are used for validation of the analysis technique presented in this article. All of the specimens were attached with specially designed cylindrical bearings to provide simple supports that allowed the specimen to rotate freely about the minor (weak) axis. The test setup was designed so that (i) the end-bearings provided simple supports to the column specimens, (ii) axial loads remained independent of the thermal expansion or contraction of the column specimens, and (iii) the temperature variation along the heated portion of the column specimen was small. A portion of the flanges of all of the specimens was heated so that a thermal gradient along the flange width was developed. SFRM fire protection was removed selectively from some portions of the specimen sections to increase the magnitude of the thermal gradient. Only the middle portion of the column specimens was subjected to heating so that the end bearings, hydraulic actuator and the loading frame were not exposed to direct heat. This is a limitation in most of the column tests at elevated temperatures. It was observed that this limitation did not affect the overall inelastic buckling behavior of the columns significantly. The testing procedure entailed the following steps:

1. A small axial load equal to 400 kN was applied initially to align the specimen. Longitudinal strain gauges installed at the column mid-

section were used to ensure the concentricity of the applied axial loading and the specimen alignment.
2. The loading was increased monotonically up to the specified value of axial load, P_u, listed in Table 1.
3. Steel temperatures were increased until inelastic column buckling occurred while the axial load was maintained. Both flanges of the specimens were partially exposed to radiant heating as shown in Fig. 1. All of the columns buckled towards the hotter side. The final permanent deflected shapes of the three specimens are also shown in Fig. 1.

FE-based heat transfer and stress analyses as described above were conducted on these columns to calculate the structural response of the system. The measured temperatures were applied as the input for the heat transfer analysis and the temperature field calculated from the heat transfer analysis, along with the applied axial loads and column self-weight, were used as input to the structural analysis. Fig. 2 shows comparisons of numerically predicted and experimentally measured axial displacement–time responses (δ–t) of the column specimens. The axial displacements of the column specimens initially decrease because the axial load is increased at ambient temperature. Then, the specimen displacements start to increase due to increasing flange temperatures. The rate of increasing axial displacements is comparable between the measured and the calculated results.

The 3D FEM column models indicate buckling approximately 10 to 15 min earlier than the actual specimens. In the tests, the stability failure was developed more gradually. This discrepancy of failure time is probably caused by the difference between the actual and the idealized σ–ε–T model used in the analysis. The finite element model including the Eurocode-3 steel properties calculates a conservative failure time of the column in fire.

3. Parametric study and results

A significant thermal gradient in the column cross-section, in addition to rendering the column weaker and less stiff, introduces an asymmetry in the column cross-section and a large geometric imperfection (bowing) in the column. These factors affect the failure mode and the load capacity of the column. Failure of simply-supported columns with four different column cross-sections (W8 × 35, W12 × 58, W14 × 90, and W14 × 159) and different slenderness and axial load values were simulated for three thermal load cases as discussed below. Although the column can have many possible combinations of heating depending upon the location of the column in the compartment, three basic cases (shown in Fig. 3) are believed to represent the most likely configurations of fire exposure to a column.

3.1. Fire loading and the results of heat transfer analysis

For the parametric study conducted on the numerical models of the columns, three different fire loading scenarios were considered (Fig. 3): (a) columns heated from all sides representing the interior columns of typical building structures, (b) columns subjected to heating on one flange and a portion of the web representing the perimeter columns of a building structure with web perpendicular to the building perimeter, and (c) columns subjected to heating on one half-side of both flanges representing the perimeter columns of a building structure with web parallel to the building perimeter. In all three cases, the steel column was protected with SFRM on all sides. The interfaces between the building walls and the column cross-section (shown in Fig. 3(b) and (c)) are assumed to provide adiabatic boundary condition. The ASTM-E119 [29] standard fire T–t relationship (used for standard fire tests in the US) was used as the thermal loading (T_g) to conduct the heat transfer analysis. Ambient temperature was assumed to be 20 °C.

The results from the heat transfer analyses of a W12 × 58 cross-section are included in Fig. 3 (a–c). The figures include the calculated nodal time–temperature histories for some of the important locations in the cross-section. As shown in Fig. 3(a), for the case of all-around heating, the difference between the temperatures at different locations of the cross-section is insignificant, and can be ignored for all practical purposes. For the case of thermal gradient along the web (Fig. 3(b)), the temperature difference between the hotter and cooler sides is more significant than in the case of thermal gradient along the flanges (Fig. 3(c)). This is due to the shape of the wide-flange cross-sections. When there is thermal gradient along the web, the only path for the heat to migrate from the hotter flange to the cooler flange is through the web. The relatively long, thin web resists heat flow from the hot flange to the cold flange producing greater temperature difference between the two flanges. Further evaluations verified that a thermal gradient along the web (Fig. 3(b)) will generally be larger than the gradient along the flanges (Fig. 3(c)).

3.2. Thermal gradient along the flanges

In order to investigate the behavior of pin-ended columns that are subjected to one sided heating such that one half of both flanges are heated, temperature histories shown in Fig. 3 (c) are used as thermal loading in the structural analysis part. Sixty four cases for each of the four wide flange shapes were analyzed with slenderness value (L/r_y) ranging from 10 to 150 and axial load varying from 20% to 100% of the ambient load capacity (P_n). Since temperature is not uniform through the cross-section, the average flange temperature has been reported as the failure temperature (T_F) for the column.

Fig. 1. Thermal loading patterns and final deflected shapes after tests.

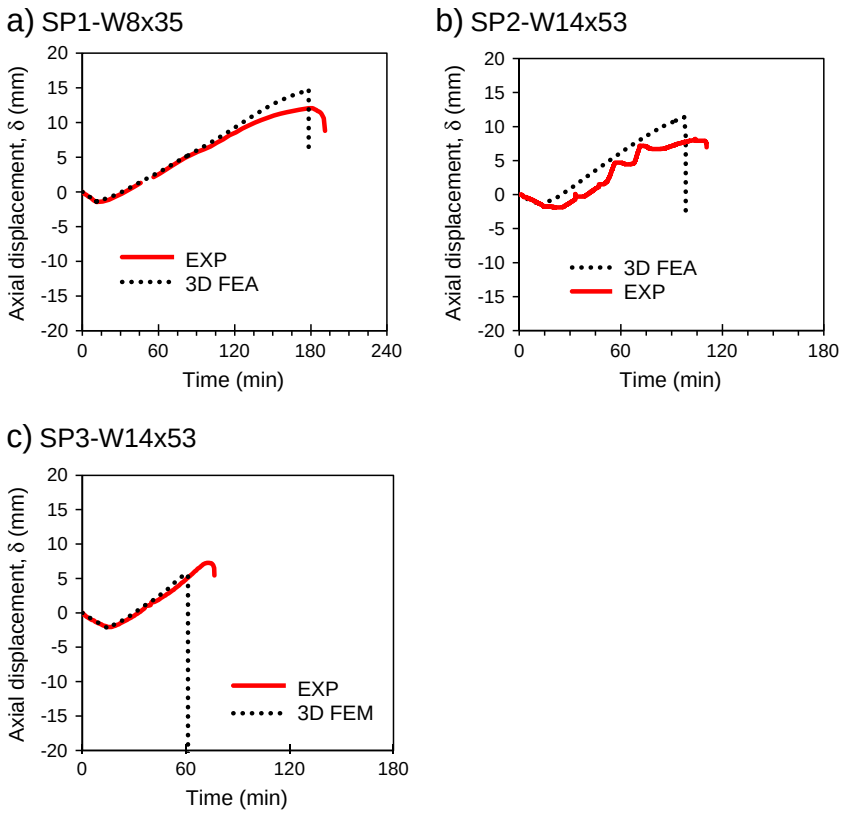

Fig. 2. Comparisons of the predicted and measured axial displacement behavior of the column specimens.

Effects of the residual stresses as well as initial imperfections, both local and global, are taken into account before loading and heating the column to failure. Initial imperfection of magnitude equal to the column length/1500 is assigned in the direction of the side exposed to fire. Table 2 shows the average flange temperatures (T_F) values for the W12 × 58 columns of various lengths for different axial load values at the time of failure. The numbers in the parentheses indicate the duration of fire (t_F) before the columns fail. Irrespective of the column length, there is always a significant moment component due to the asymmetry in the section properties. Therefore, complete section plastification corresponding to squash load capacity is never observed. All the columns with thermal gradient along the flanges failed due to flexural buckling about the weak axis followed by local buckling of the web and the flanges under the combined axial load and moment effects. Some of the columns bent towards the hotter side of the cross-section and some of the columns bent towards the cooler side of the cross-section. Table 2 also highlights the columns that bent towards the cooler side (hotter side yielded in compression). It can be observed that slender columns were more likely to bend towards the hotter side, whereas the columns having higher failure temperature (smaller axial load) failed by bending towards the cooler side of the cross-section. Fig. 4 presents the deformed shapes for the two cases.

3.2.1. Mechanism of failure

As discussed earlier and explained by Garlock and Quiel [14], due to uneven material stiffness through the cross-section, the effective centroid shifts towards the cooler (stiffer) side. As shown in Fig. 5, this shift is the distance e_1 from the geometric centroid of the section. If the column is loaded concentrically, i.e., the axial load is acting at the geometric centroid, the moment corresponding to the shift of the effective centroid causes the column to bend towards the cooler side. However, bowing of the column, produced by uneven expansion of the section, makes the mid-section bow towards the hotter side of the column by e_2 with respect to the line of action of the applied load. The actual direction of bending, therefore, will be governed by the larger of the two values. It can be observed from Table 2 that either mode can control column failure behavior in large ranges of slenderness and temperature values, respectively, and both effects should be considered in design equations. Table 2 also shows two distinct trends: (1) slender columns are more likely to bend towards hotter side (i.e., cooler side fails in compression) and stub columns were more likely to bend towards the cooler side (i.e., hotter side fails in compression), and (2) columns loaded with a smaller fraction of their ambient load capacity are more likely to bend towards the cooler side. The following paragraphs offer qualitative explanations for these observations.

Slender columns are more likely to bend towards the hotter side, i.e., bowing effect governs the column behavior for slender columns. Assuming that the temperatures do not change along the length of the column and there are no axial loads or restraints acting on the column, thermal gradient across the section produces a uniform curvature ϕ_b due to bowing effects. Therefore, the displacement of the mid span due to bowing effect would be equal to $\delta_b = [1 - \cos(\phi_b L/2)]/\phi_b \approx \phi_b L^2/8$ where L is the length of the column. Therefore, as the length of the column increases, the bowing effect increases more rapidly. The shift in the effective centroid of the cross-section is a function of the temperature distribution, which is independent of the column length. Thus, it can be inferred that, for very short columns, the bowing effect is insignificant and the behavior is governed by the shift in the location of the effective centroid. For more slender columns, however, the behavior is governed by the bowing effect, which is why longer columns tend to bend towards the hotter side.

Table 2 also shows the trend that the effect of the asymmetry in the cross-section, i.e., shift of the effective centroid, increases in columns with higher temperatures. This is consistent with the observations of Garlock and Quiel [14]. For a W-shaped cross-section with uniform material properties, the effective centroid coincides with the geometric centroid. As the asymmetry in the material properties increases, the

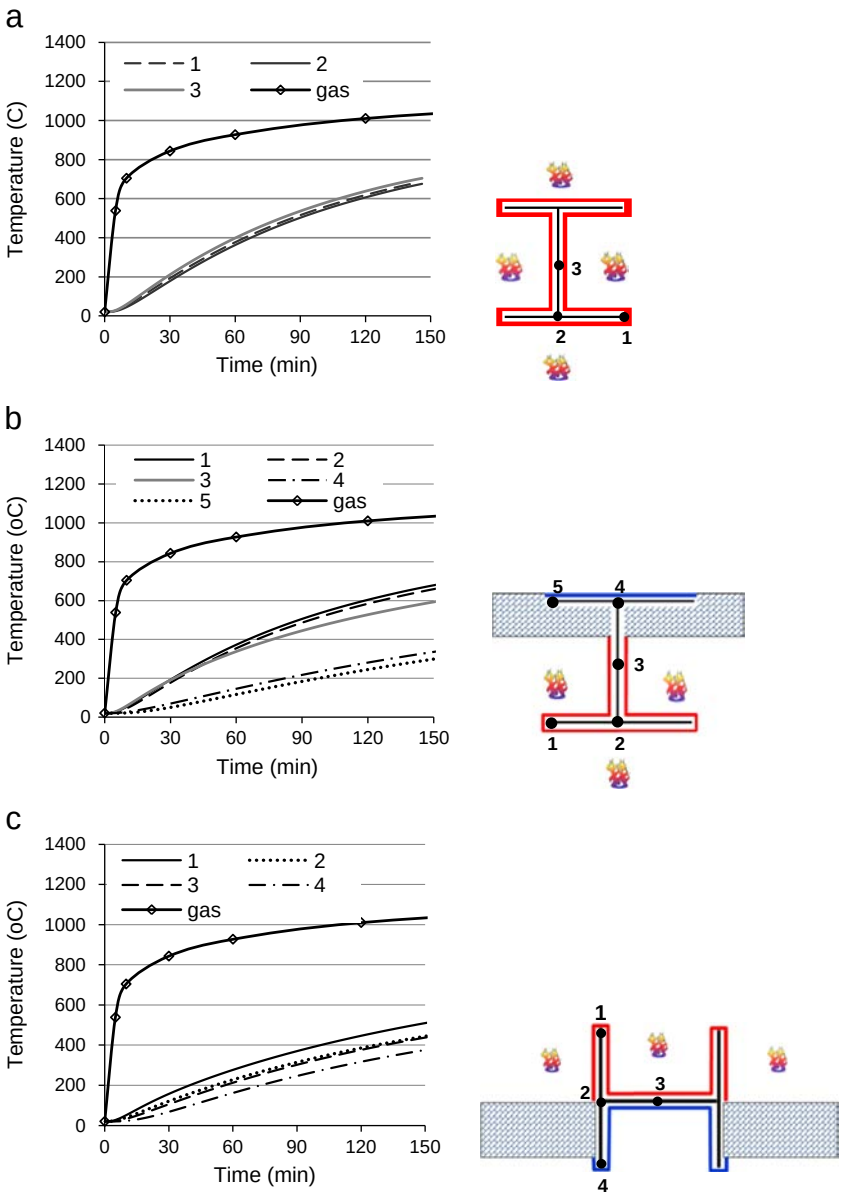

Fig. 3. Temperatures at different locations across the section of W12x58 columns for (a) uniform heating, (b) gradient along the web, and (c) gradient along the flanges.

effective centroid moves farther away from the geometric centroid. Consider a W-shape steel section where the difference between the temperatures of the hotter and the cooler sides is maintained as the overall temperature of the section is increased. Fig. 6 plots the ratios of (a) elastic moduli and (b) yield strengths, at the two ends of a section versus the temperature at the hotter end of the section. Each curve in these graphs represents a constant temperature difference of 100 °C, 200 °C, or 300 °C, respectively between the hotter and the cooler side. These plots have been developed using the structural steel material properties at elevated temperatures as prescribed by the Eurocode-3 [3]. As the eutectic phase change takes place at 723 °C for steel, data points beyond 723 °C may not be accurate. Fig. 6 indicates that the ratio of elastic moduli and the ratio of the yield stresses at the two ends keep increasing until the maximum temperature in the cross section reaches at least 700 °C. These trends imply that, for most of the relevant temperature range, the asymmetry in a cross-section keeps õincreasing (i.e., the effective centroid shifts father from the geometric centroid) as the average temperature of the section increases, while the difference between the maximum and minimum temperatures remains constant. This explains why the behavior of columns failing at higher temperatures is more likely to be governed by the shift in the effective centroid than the bowing effect.

Table 2
Failure temperatures (T_F) and failure time (t_F) for W12 × 58 column with thermal gradient along the flanges.

W12x58		0.9 P_n^{20}	0.8 P_n^{20}	0.7 P_n^{20}	0.6 P_n^{20}	0.5 P_n^{20}	0.4 P_n^{20}	0.2 P_n^{20}
λy	P_n^{20} (kN)	Failure temperature (°C) and time of failure (minutes)						
10	3740	428 (142)	450 (154)	492 (179)	528 (203)	562 (230)	599 (264)	697 (407)
30	3520	181 (48)	301 (88)	448 (153)	493 (179)	527 (202)	565 (233)	665 (350)
40	3230	153 (41)	235 (65)	335 (100)	462 (161)	534 (208)	564 (232)	660 (342)
50	2930	109 (30)	199 (54)	288 (83)	384 (121)	490 (178)	574 (241)	657 (336)
60	2670	54 (15)	148 (39)	227 (62)	321 (95)	427 (142)	523 (200)	662 (345)
80	2160	35 (9)	68 (18)	150 (40)	225 (62)	325 (97)	444 (151)	613 (278)
100	1690	31 (9)	48 (13)	92 (25)	179 (48)	268 (76)	379 (118)	588 (253)
150	859	35 (9)	53 (15)	88 (24)	165 (44)	256 (72)	359 (110)	573 (240)

Shaded cells mark the columns that bend towards cooler side. All other columns bend towards hotter side.

3.3. Thermal gradient along the web

The heating configuration shown in Fig. 3 (b) is used to develop the thermal gradient along the web of the column. The *T–t* histories

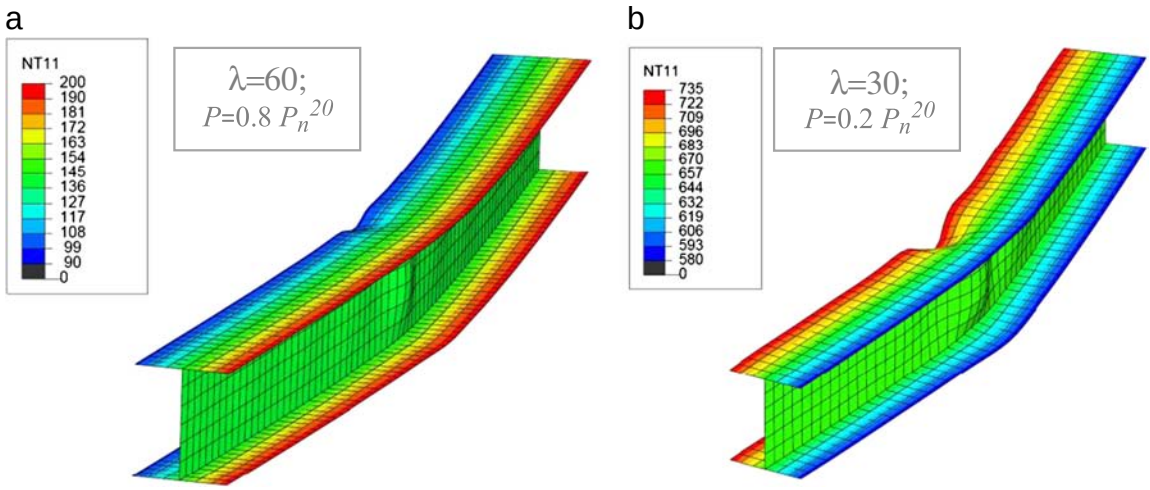

Fig. 4. Deformed shapes of W12 × 58 columns bending towards (a) hotter side and (b) cooler side when subjected to thermal loading with thermal gradient along the flanges.

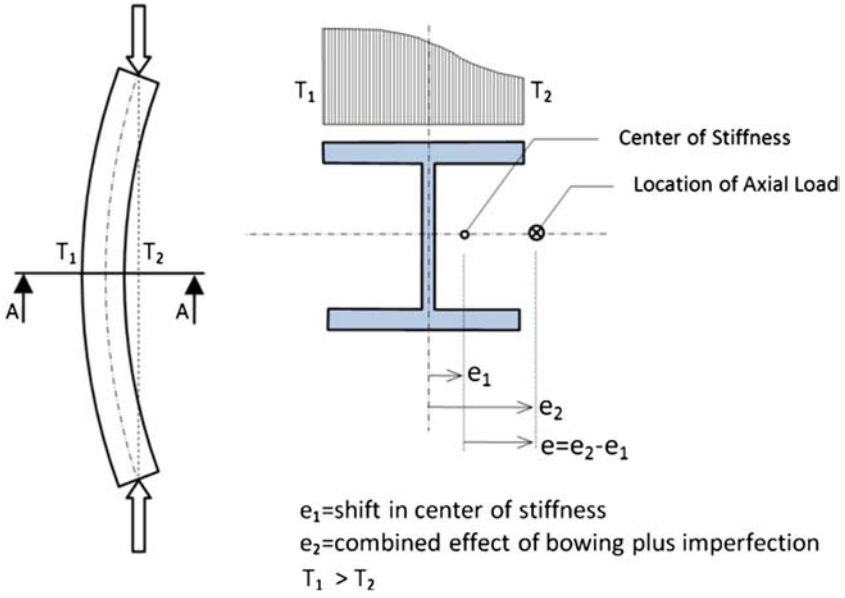

Fig. 5. Net eccentricity in the column section with gradient.

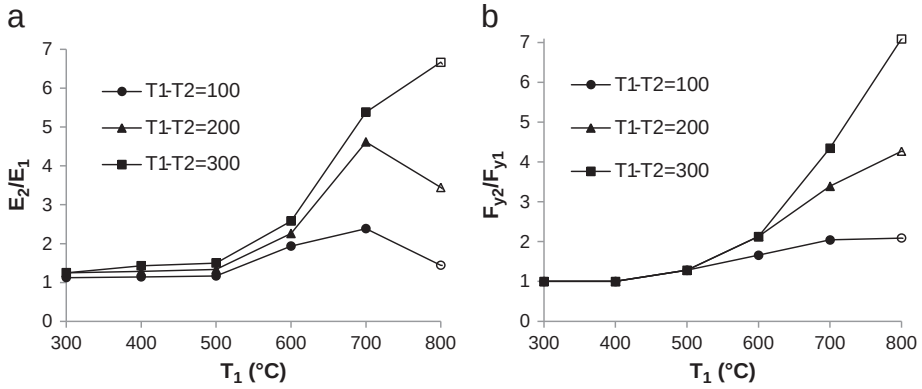

Fig. 6. Ratio of (a) elastic moduli and (b) yield strengths at the two ends of a column cross-section as the temperature of the cross-section increases while the difference of the temperature at the two ends (T_1–T_2) is maintained at 100, 200 and 300 °C, respectively.

Table 3
Failure temperatures (T_F) and failure time (t_F) for a W12 × 58 column with a thermal gradient along the web.

W12x58		0.9 P_n^{20}	0.8 P_n^{20}	0.7 P_n^{20}	0.6 P_n^{20}	0.5 P_n^{20}	0.4 P_n^{20}	0.2 P_n^{20}
λy	P_n^{20} (kN)	Failure temperature (°C) and time of failure (minutes)						
10	3740	319 (82)	342 (89)	368 (98)	397 (109)	425 (120)	463 (137)	567 (207)
30	3520	230 (56)	318 (81)	355 (93)	385 (104)	415 (116)	450 (131)	551 (193)
40	3230	169 (41)	294 (74)	358 (94)	395 (108)	424 (119)	461 (136)	564 (205)
50	2930	171 (41)	273 (67)	350 (91)	397 (109)	431 (122)	470 (141)	577 (216)
60	2670	162 (39)	250 (61)	337 (87)	389 (106)	437 (126)	478 (144)	590 (226)
80	2160	160 (39)	240 (59)	316 (81)	379 (100)	432 (123)	491 (151)	639 (261)
100	1690	153 (37)	239 (58)	310 (79)	373 (100)	423 (119)	484 (147)	691 (302)
150	859	171 (42)	258 (63)	327 (84)	376 (101)	415 (116)	460 (136)	600 (233)

Shaded cells mark the columns that fail in inelastic flexural-torsional buckling mode.

Table 4
Failure temperatures (T_F) and failure time (t_F) for W12 × 58 column with uniform temperature distribution.

W12x58		0.9 P_n^{20}	0.8 P_n^{20}	0.7 P_n^{20}	0.6 P_n^{20}	0.5 P_n^{20}	0.4 P_n^{20}	0.2 P_n^{20}
λy	P_n^{20} (kN)	Failure temperature (°C) and time of failure (minutes)						
10	3740	265 (41)	440 (73)	492 (84)	531 (94)	567 (104)	607 (116)	703 (148)
30	3520	185 (29)	298 (46)	441 (73)	505 (88)	545 (98)	585 (109)	686 (145)
40	3230	182 (28)	267 (41)	385 (61)	478 (81)	530 (94)	572 (105)	679 (142)
50	2930	182 (28)	261 (40)	347 (54)	444 (75)	517 (90)	561 (103)	670 (139)
60	2670	171 (27)	241 (37)	324 (50)	413 (66)	506 (88)	551 (99)	660 (134)
80	2160	167 (26)	234 (36)	300 (47)	374 (59)	472 (80)	538 (96)	650 (131)
100	1690	167 (26)	239 (37)	298 (47)	363 (58)	461 (77)	537 (96)	647 (129)
150	859	207 (32)	288 (44)	353 (56)	420 (68)	522 (92)	564 (103)	674 (140)

Shaded cells mark the cases where designing for all around heating would be unconservative if columns were heated so that there was a thermal gradient along the flanges.

obtained from the 2-D heat transfer analysis of the column cross-section are used for simulating the structural behavior of the column. Except for the T–t histories shown in Fig. 3(b), modeling approach (including member dimensions, geometric modeling, procedure of the analysis, and the loading sequence) remains the same as in the structural analysis of columns with a thermal gradient along the flanges. Like the case of the thermal gradient along the flanges, four different column cross-sections of different lengths and different applied axial loads were analyzed to failure. The average of the flange temperatures at the time of failure was reported as failure temperature (T_F) of the column.

Values of failure temperature (T_F) and the corresponding mode of failure for the W12 × 58 columns of different lengths and load values are summarized in Table 3. The numbers in the parentheses indicate the duration of fire (t_F) before the columns fail. Unlike the case of a thermal gradient along the flanges, the failure mode for these columns is not restricted to flexural buckling. Due to the lack of symmetry about the strong axis of the column cross-section, two different modes of failure are observed. Some of the columns (shaded cells in Table 3) fail by inelastic flexural-torsional buckling that involves flexure about the weak axis and torsion about the longitudinal axis (Fig. 7 (b)); the rest of the columns fail by inelastic flexural buckling about the strong axis (Fig. 7 (a)). Columns failing in inelastic flexural buckling about the strong axis are observed to bend towards the cooler side of the cross-section, i.e., the hotter flange yields in compression. Considering the large number of columns undergoing flexural-torsional buckling, it is evident that the flexural buckling mode alone does not adequately capture the stability behavior of columns with thermal gradient along the web. The effects of the torsional component in the failure modes of these columns should not be ignored.

3.3.1. Mechanism of failure

The pattern of the shaded cells in Table 3 indicates that slender columns are more likely to undergo inelastic flexural-torsional buckling, whereas shorter columns are more likely to fail due to inelastic flexural buckling about the strong axis. This observation is analogous to the behavior of beams carrying bending moments in the strong axis direction. The capacity of a beam with shorter unbraced length is governed by the limit state of yielding in flexure about the strong axis but the capacity of a beam with longer unbraced length is governed by the limit state of lateral torsional buckling.

3.4. Uniform temperature versus thermal gradient

Although the thermal gradient in a column heated from one side contributes to bowing of the column and asymmetry in the section stiffness, the net heat influx into the column remains less than that for a column engulfed by fire from all sides. Therefore, it is not obvious whether the net effect of the thermal gradient would reduce or increase the load carrying capacity of the column. Failure temperatures for columns with uniform thermal loading following the T–t curves shown in Fig. 3(a) are presented in Table 4. The numbers in the parentheses indicate the duration of fire (t_F) before the columns fail. On comparison of the values of t_F for the three types of thermal loading, one observes that all the columns subjected to thermal gradient along the web fail later than columns subjected to uniform heating. However, when subjected to a thermal gradient along the flanges, some columns (very slender columns with a large axial load ratio) fail sooner than they fail when subjected to all around heating. These columns are marked by shaded cells in Table 4. This clearly indicates that, there may be combinations of loads, slenderness values and thermal loading patterns (non-uniform) for which the assumption of uniform thermal loading will lead to unsafe column design.

4. Proposed design equations

The observations from the parametric study discussed above are used to develop design equations for columns with thermal gradients at elevated temperatures. When thermal gradient is applied to a straight

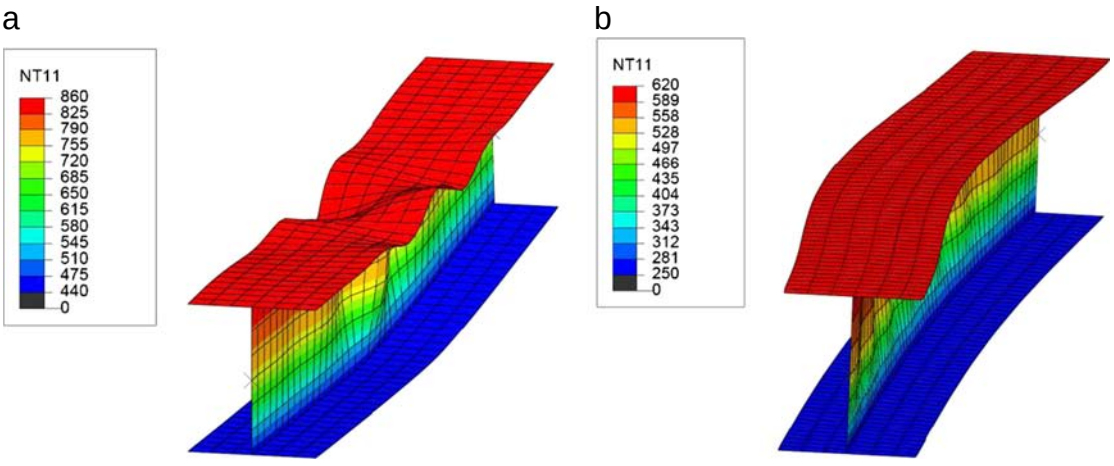

Fig. 7. Deformed shapes of W12 × 58 columns with thermal gradient along the web failing in (a) inelastic flexural buckling about the strong axis and in (b) inelastic flexural-torsional buckling.

W-shape column, the column becomes a beam-column with an asymmetric cross-section and significant geometric imperfection, giving rise to second-order moments. The second-order moments require that the column (designed as a pure compression member at ambient temperature) be evaluated as a beam column at elevated temperatures. The proposed design method is similar to the existing AISC beam-column design equation at ambient temperature. The proposed equation is calibrated using the parametric study conducted on W12 × 58 columns and is verified against other column cross-sections, namely, W8 × 35, W14 × 90, and W14 × 159.

The load capacity of the column, P_n^T, will be given by the Eq. (6). Where, δ_e and δ_b are deflections at the mid span due to the asymmetry of the section and bowing effects, given by Eqs. (7) and (8), respectively. P_{sf}^T is the load capacity of a hypothetical straight column that has same length, cross-section, and temperature distribution as the actual column, without including the effects of the second-order moments due to bowing or the shift in the effective centroid of the column. M_n^T is the nominal moment capacity of the column in the direction of the thermal gradient. In Eq. (8), $(\Delta l/l)_{hot}$ and $(\Delta l/l)_{cold}$ are the thermal strains calculated at the hotter and cooler ends of the cross-section, respectively. These are to be calculated using the thermal elongation coefficients for steel as prescribed by the Eurocode-3 [3]. In Eqs. (7) and (8), L is the length of the simply supported column. If the thermal gradient is applied along the web, d will be equal to the depth of the wide-flange section. If the thermal gradient is applied along the flanges, d will be taken as the flange width of the wide-flange section. In Eq. (7), y_{NA} is the distance of the elastic neutral axis from the hotter end of the cross-section in the direction of the thermal gradient. For calculation of the neutral axis location, strong axis bending should be considered for thermal gradient along the web, and weak axis bending should be considered for thermal gradient along the flanges. As shown in Fig. 8, $(I)^T$ is the second moment of the effective area (A^T) of the cross-section calculated about the neutral axis discussed above. E is the elastic modulus of steel at ambient temperature.

$$\frac{P_n^T}{P_{sf}^T}+\frac{P_n^T(\delta_b-\delta_e)}{M_n^T\left(1-\frac{P_n^T}{P_e^T}\right)}=1 \quad ; \qquad \text{and } P_n^T \le P_{sf} \tag{6}$$

$$\delta_e=\frac{P_n^T\left(y_{NA}-{}^{d}/_{2}\right)L^2}{8E(I)^T} \tag{7}$$

$$\delta_b=\frac{[(\Delta l/l)_{hot}-(\Delta l/l)_{cold}]L^2}{8d} \tag{8}$$

$$P_{sf}^t=\begin{cases}\left[0.658^{\frac{P_{yc}^T}{P_e^T}}\right]P_{yc}^T & \text{for } P_e^T \ge 0.44P_{yc}^T\\ 0.877P_e^T & \text{for } P_e^T < 0.44P_{yc}^T\end{cases} \tag{9}$$

Eq. (9), to be used for the calculation of P_{sf}^T, is the same as the AISC 360 [1] column capacity equations for the flexural buckling limit state of a compression member (E3-2 and E3-3) with the following modifications. P_e^T in Eq. (9) is the elastic buckling load of the equivalent straight column. The shift in the elastic neutral axis $(y_{NA}-{}^{d}/_{2})$, the moment of inertia $(I)^T$ of the equivalent elastic section, and P_e^T is calculated by taking into account the reduction in the modulus of elasticity of steel due to temperature change as shown in Fig. 8. P_{yc}^T in Eq. (9) is the compressive strength of a stub column that has the same cross-section and temperature distribution as the actual column. As explained below, the method to calculate P_{yc}^T is different from the stub column capacity (P_y^T) calculated for uniformly heated column or ambient temperature columns.

Due to the uneven temperature distribution through the cross-section, the yield stresses at the hotter side are lower than the yield stresses at the cooler side of the cross-section. As a result, the effective centroid shifts towards the cooler end of the cross-section. If the load was applied at the effective centroid of the cross-section, the entire cross-section would reach its full plastic capacity at the time of failure. However, because the external load is applied at the geometric centroid of the column cross-section, only the hotter side of the column will yield. In order to maintain section equilibrium, the cooler half of the cross-section will not reach its maximum plastic capacity. The internal force in the hotter half of the cross-section can be calculated by integrating the yield stresses in that portion. The internal forces in the cooler half should ideally be calculated by enforcing strain compatibility and section equilibrium, which can be a cumbersome process. A simplistic assumption can be made that the internal stress distribution in the cooler half is a mirror image of the internal stress distribution in the hotter half, which will automatically satisfy moment equilibrium.

Fig. 9 illustrates this difference between P_y^T and P_{yc}^T. P_y^T is equal to the force calculated by integrating the temperature dependent yield stresses through the column cross-section, whereas P_{yc}^T is equal to two times the force calculated by integrating the temperature dependent yield stresses of the hotter half of the cross-section. This assumption provides a good approximation of the P_{yc}^T value. For example, using the finite element method discussed in Section 2.2, the compressive strength of a W8 × 35 stub column (0.52 m long, $L/r_y = 10$) with thermal gradient along the flanges (T_{max} = 675 °C, T_{min} = 525 °C) is estimated to be equal to 870 kN. In comparison, using the assumption discussed above, P_{yc}^T value for this column is calculated to be approximately equal to 860 kN while P_y^T is approximately equal to 1100 kN.

$$M_n^T=\begin{cases}M_p^T & \text{when thermal gradient is along the flanges or (thermal gradient along the web and } L<L_p)\\ C_b\left[M_p^T-\left(M_p^T-0.7F_{y,hot}S_{x,hot}\right)\left(\frac{L-L_p}{L_r-L_p}\right)\right] \le M_p^T & \text{thermal gradient is along the web and } L_p \le L<L_r\\ \frac{C_b\pi^2E_{,hot}}{\left(\frac{L}{r_t}\right)^2}\sqrt{1+0.078\frac{J}{S_{x,hot}\,h_o}\left(\frac{L}{r_t}\right)^2} \le M_p^T & \text{thermal gradient is along the web and } L \ge L_r\end{cases} \tag{10}$$

where

$$L_p=1.1\ r_t\sqrt{\frac{E_{,\ hot}}{F_{y,\ hot}}} \tag{11}$$

$$L_r=1.95\,r_t\frac{E_{,hot}}{0.7F_{y,hot}}\sqrt{\frac{J}{S_{x,hot}\,h_o}}\sqrt{1+\sqrt{1+6.76\left(\frac{0.7F_{y,\ hot}}{E_{,hot}}\frac{S_{x,hot}\,h_o}{J}\right)^2}} \tag{12}$$

$$r_t=\frac{b_{f,hot}}{\sqrt{12\left(1+\frac{h_c\,t_w}{6b_{f,hot}\,t_{f,hot}}\right)}} \tag{13}$$

M_n^T is the nominal flexural capacity of the column in the direction of the thermal gradient with no axial load applied. Calculation of M_n^T is based on the AISC flexural design provisions for asymmetric beam cross-sections. If the member has a thermal gradient along the flanges, flexural yielding about the weak axis is the only applicable limit state; therefore M_n^T will be equal to M_p^T, the plastic moment capacity about the weak axis. If the member has thermal gradient along the web, it will introduce bending moment about the strong axis. Applicable limit states are (1) flexural yielding about the strong axis and (2) lateral-torsional buckling. For flexural yielding, the nominal moment capacity is equal to the plastic moment capacity about the strong axis, which is independent of the moment direction (hot flange in compression or

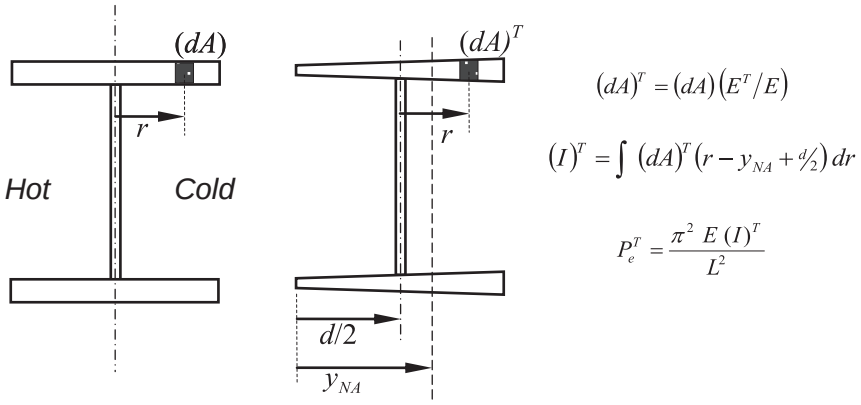

Fig. 8. Effective elastic cross-section with thermal gradient and calculation of the elastic buckling load for the column.

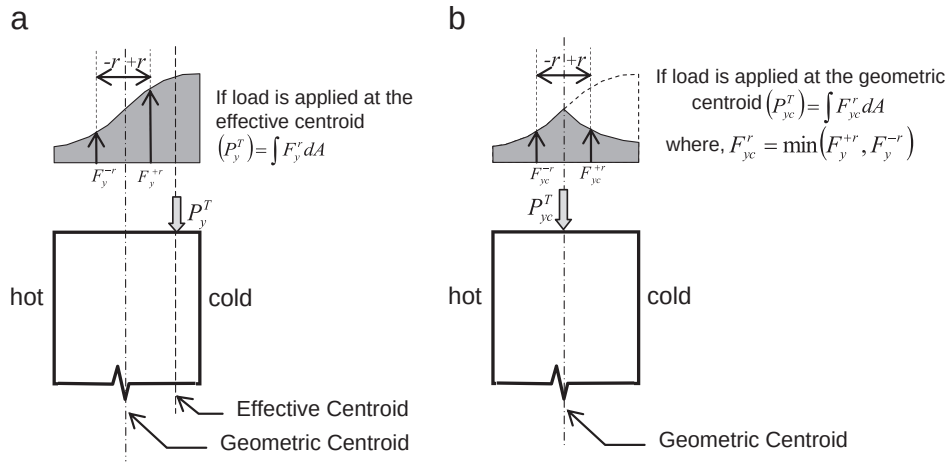

Fig. 9. Strength of a stub column with thermal gradient if (a) loaded at the effective centroid, and if (b) loaded at the geometric centroid.

cold flange in compression). However, in the case of flexural-torsional buckling, the moment capacity depends on the lateral stiffness of the flange in compression. From the FEM simulations, it has been observed that in cases where flexural torsional buckling mode dominates, it is always the hot flange that buckles laterally. Also, because the hotter flange has lower stiffness, it is conservative to assume that the direction of the moment is such that it applies compression on the hotter flange. Therefore, for the calculation of M_n^T, the hotter flange is assumed to be in compression and the cooler flange in tension. Flexural strength, M_n^T, is calculated using Eqs. (10) to (13). Examples of how to use these design equations for a column in all three basic heating configurations have been presented by Agarwal [30].

5. Verification of proposed design equations

The proposed design equations were validated against experimental data reported by Choe [23] as well as detailed FEM based simulations conducted on several column sizes. Fig. 10 shows the experimentally measured temperatures across the sections of column specimens at failure, and the measured axial load capacity of the column specimens are reported in Table 1. These measured temperature values were used to calculate the axial capacity of the column specimens using the proposed Eqs. (6) to (13). The calculated capacities of the specimens SP1-W8 × 35, SP2-W14 × 53, and SP3-W14 × 53 were 900 kN, 1570 kN and 1480 kN, respectively. These calculated values are approximately 13%, 8%, and 2% greater than the respective column capacities measured during the tests. These discrepancies are potentially due to the unintended temperature variations along the specimen length during the test (Choe [23]). The temperature values shown in Fig. 10 were averaged values of the temperatures recorded by several thermocouples located at the heated sections along the column length. The column capacities calculated using the proposed equations compared reasonably well with test data.

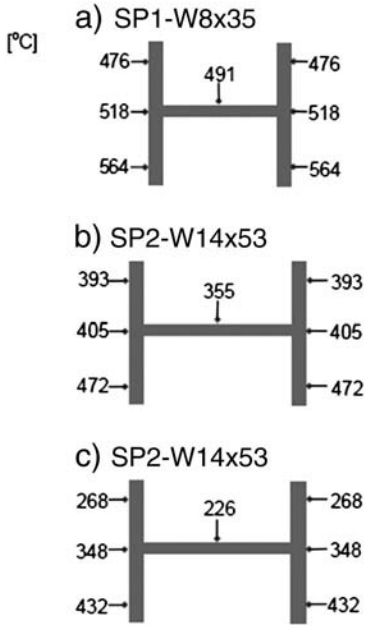

Fig. 10. Measured temperatures of the column specimens exposed to uneven heating.

In addition to the experimental tests, 3D FEM simulations of columns with various cross-section dimensions, slenderness values, and temperature distributions were conducted to validate the proposed equations. As mentioned in the previous section, the proposed equations were calibrated using the parametric study conducted on W12 × 58 columns. Structural wide flange shapes W8 × 35, W14 × 90, and W14 × 159 were selected for the FEM-based validation study. Fig. 11 compares the load capacities calculated using the proposed design equations and the results from the FEM simulations. The graphs in Fig. 11 plot the axial load capacity as a function of the column slenderness (L/r_y). The temperature values indicated in each plot are the average flange temperature at the time of failure. The axial load capacity calculated using the proposed equation (P_n) compares reasonably with the simulated data (P_{FEM}) for the test cases involving wide range of sections, temperatures, and slenderness values. The numerical ratios of P_{FEM}/P_n vary from 0.9 to 1.6 with an overall average value of 1.10 and coefficient of variation of 0.07. The limit state of local buckling is not included in the proposed equations but is included directly in the 3D finite element analysis. Further research should be conducted to include this limit state in the design equation, particularly for the case of stub columns with thermal gradients along the webs.

6. Summary and conclusions

Thermal gradients in a column cross-section can reduce the load carrying capacity for two reasons: (1) column deformations due to uneven thermal expansion (bowing) and (2) asymmetry in the column cross-section due to uneven degradation of material properties (yield stress and elastic modulus). Many researchers have discussed these effects and some researchers have also proposed design methods for calculating the load carrying capacity of such columns. The goal of the research presented in this paper was to develop design equations for columns exposed to uneven heating by addressing additional limit states. Both experimental and numerical studies using the finite element method were conducted to develop and verify the column design equations. The simulations included three different thermal loading cases such as uniform heating, thermal gradient along the flanges, and thermal gradient along the web. ABAQUS [25] was used for simulating the heat transfer as well as the dynamic structural response of columns. The heat transfer analysis procedure included all three effects of conduction, convection, and radiation. The time–temperature field obtained from the heat transfer analysis was applied as a thermal loading to the 3D structural models. Simply supported W-shaped columns of various lengths and cross-sections were loaded to different axial load values and heated to failure.

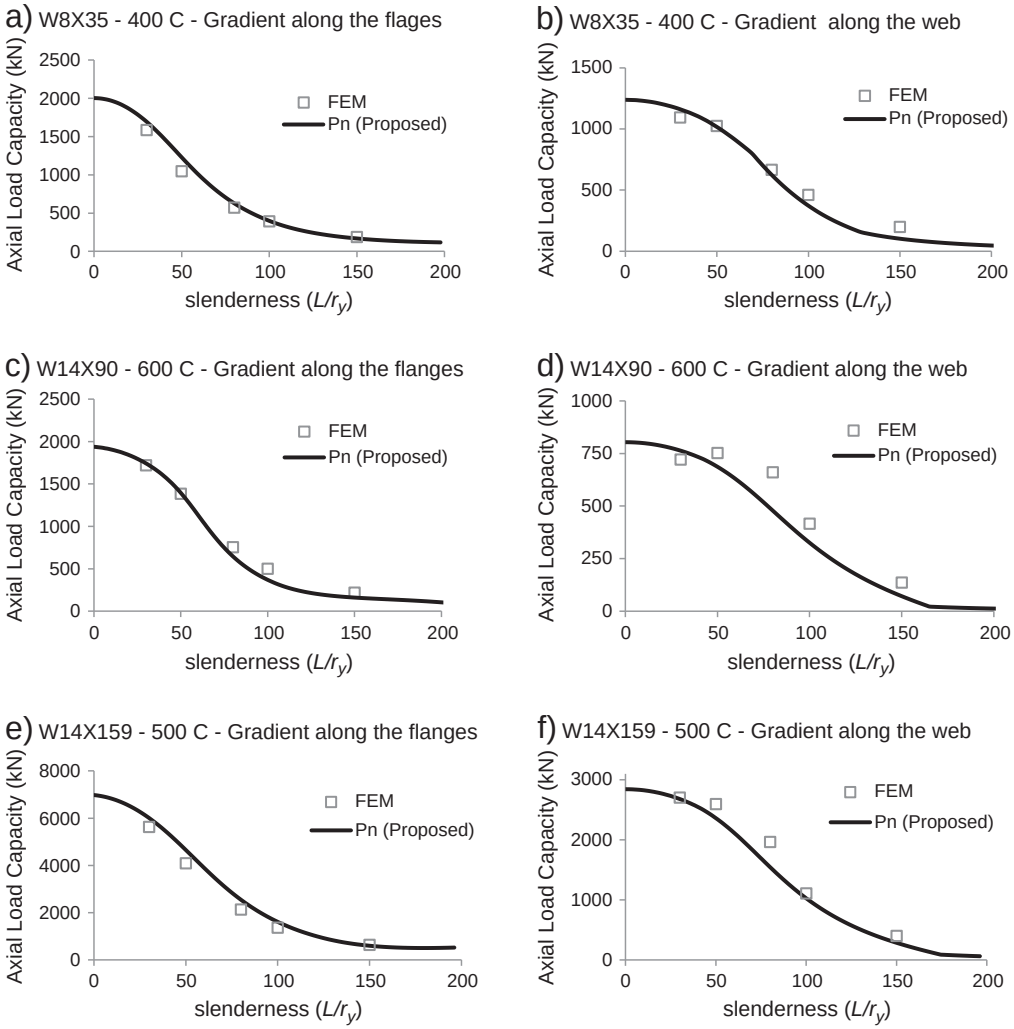

Fig. 11. Comparison of the results from the FEM based simulations with the proposed design equation for W8 × 35 column at 400 °C average flange temperature with thermal gradient (a) along the flanges, and (b) along the web, W14 × 90 column at 600 °C average flange temperature with thermal gradient (c) along the flanges and (d) along the web, and for W14 × 159 column at 500 °C average flange temperature with thermal gradient (e) along the flanges, and (f) along the web, respectively.

From this parametric study, the following important observations are drawn.

- Columns subject to uniform heating have much larger heat influx and, therefore, have a higher average temperature than columns exposed to uneven heating.
- In most cases, uniformly heated columns reached their respective critical temperature sooner than the partially heated columns. All the columns except very slender columns that were loaded with more than 50% of their ambient load capacity failed sooner when heated from all sides.
- A column with thermal gradient along the flanges always buckled about the weak axis. A slender column is more likely to bend towards the hotter side. However, a stockier column subjected to a small axial load is likely to bend towards the cooler side before failure.
- A column with thermal gradients along the web can buckle about the strong axis or in the flexural-torsional mode involving flexure about the weak axis and torsion. A slender column is more likely to fail in the flexural torsional buckling mode than a stockier column.
- Using the failure temperature values obtained from the analyses, a set of design equations was proposed. The proposed equations quantify the effects of bowing, asymmetry in the column cross-section, and the corresponding secondary moment effects.
- The proposed equations compare reasonably with the results from the finite element based simulations and the full-scale test data.
- The effects of local buckling at elevated temperature are included in the finite element analyses, but further research is required to include these effects in design equations, particularly for the case of stub columns with thermal gradients along the webs.

This paper presented a detailed study on the behavior of wide-flange steel columns at elevated temperatures with thermal gradient in the cross-section. Further research is required to develop similar design guidelines for steel and composite beams with thermal gradient.

References

[1] American Institute of Steel Construction. ANSI/AISC 360–10: specification for structural steel buildings. Chicago, IL: American Institute of Steel Construction, Inc.; 2010.
[2] Takagi J, Deierlein GG. Strength design criteria for steel members at elevated temperatures. J Constr Steel Res 2007;63(8):1036–50.
[3] European Committee for Standardization. EN 1993-1-2: design of steel structures, part 1–2: general rules — structural fire design. Brussels, Belgium: European Committee for Standardisation; 2005.
[4] Agarwal A, Varma AH. Design of steel columns at elevated temperatures due to fire: effects of rotational restraints. Eng J AISC 2011:297–314.
[5] Talamona D, Franssen JM, Schleich JB, Kruppa J. Stability of steel columns in case of fire: numerical modeling. J Struct Eng ASCE 1997;123(6):713–20.
[6] Magnusson SE, Thelandersson S. Temperature–time curves of complete process of fire development. Theoretical study of wood fuel fires in enclosed spaces, Civil Engineering and Building Construction Series 65. Acta Polytechnica Scandinavica; 1970.
[7] Babrauskas V. COMPF2: a program for calculating post-flashover fire temperatures. NBS technical note 991. National Bureau of Standards; 1979.
[8] Franssen JM. A comparison between the parametric fire of Eurocode 1 and experimental tests. Proceedings of the Sixth International Symposium of Fire Safety Science; 1999.
[9] Lie TT. Fire temperature-time relations, chapter 4–8. SFPE handbook of fire protection engineering. 2nd ed. Society of Protection Engineers; 1995.
[10] European Committee for Standardization. EN 1991-1-2: actions on structures, part 1–2: general actions — actions on structures exposed to fire. Brussels, Belgium: European Committee for Standardisation; 2005.
[11] Olawale AO. Collapse behavior of steel columns in fire. [Ph.D. Thesis] University of Sheffield; 1988.
[12] Garlock MEM, Quiel SE. Plastic axial load and moment interaction curves for fire exposed steel sections with thermal gradients. J Struct Eng ASCE 2008;134:874–80.
[13] Antonio MC, Joao PCR, Valdir PS. Numerical study on the behavior of steel columns embedded on brick walls subjected to fire. Proceedings of International Symposium on Steel Structures: Culture and Sustainability; 2010.
[14] Garlock MEM, Quiel SE. Mechanics of wide-flanged steel sections that develop thermal gradients due to fire exposure. Int J Steel Struct KSSC 2007;7:153–62.
[15] Olesen FB. Fire tests on steel columns. Aalborg, Denmark: Institute of Building Technology and Structural Engineering; 1980.
[16] Vandamme M, Janss J. Buckling of axially loaded steel columns in fire conditions. IABSE Periodica, 3; 1981. p. 82–95.
[17] Aasen B. An experimental study on columns' behavior at elevated temperatures. Research report, division of steel structures. Norway: Univ. of Trondheim; 1985.
[18] Janns J, Minne R. Buckling of steel columns in fire conditions. Fire Saf J 1982;4(4):227–35.
[19] Franssen JM, Talamona D, Kruppa J, Cajot LG. Stability of steel columns in case of fire: experimental evaluation. J Struct Eng ASCE 1998;124(2):158–63.
[20] Quiel S, Garlock MEM. Closed-form prediction of the thermal and structural response of a perimeter column in a fire. Open Constr Build Technol J 2010;4:64–78.
[21] Dwaikat MMS, Kodur VKR, Quiel SE, Garlock MEM. Experimental behavior of steel beam-columns subjected to fire-induced thermal gradients. J Constr Steel Res 2011;16(1):30–8.
[22] Dwaikat MMS, Kodur VKR. Strength design criteria for steel beam-columns with fire induced thermal gradients. Eng J AISC 2011:127–40.
[23] Choe L. Structural mechanics and behavior of steel members under fire loading. [Ph.D. Thesis] Purdue University; 2011.
[24] Choe L, Varma AH, Agarwal A, Surovek A. Fundamental behavior of steel beam-columns and column under fire loading: experimental evaluation. J Struct Eng ASCE 2011;137:954–66.
[25] Hibbitt, Karlsson, and Sorenson, Inc. ABAQUS/standard version 6.9 user's manuals. Pawtucket, RI: Hibbitt, Karlsson & Sorensen, Inc.; 2009.
[26] Ruddy JL, Marlo JP, Loannides SA, Alfawakhiri F. Fire resistance of structural steel framing — AISC steel design guide 19. Chicago: AISC; 2003.
[27] Wong MB. Size effects on temperatures of structural steel in fire. J Struct Eng ASCE 2005;131(1):16–20.
[28] Cedeno G, Varma AH, Agarwal A. Behavior of floor systems under realistic fire loading. Proceedings of the ASCE Structures Congress; 2009.
[29] ASTM International. E119: standard methods of fire test of building construction and materials. West Conshohocken, PA: ASTM International; 2008.
[30] Agarwal A. Stability behavior of steel building structures in fire conditions. [Ph.D. Thesis] Purdue University; 2011.